Extreme Mechanics Letters 8 (2016) 78–87

Contents lists available at ScienceDirect

Extreme Mechanics Letters

journal homepage: www.elsevier.com/locate/eml

Large increase in stretchability of organic electronic materials by encapsulation

Eric J. Sawyer, Aliaksandr V. Zaretski, Adam D. Printz, Nathaniel V. de los Santos, Alejandra Bautista-Gutierrez, Darren J. Lipomi *

Department of NanoEngineering, University of California, San Diego, 9500 Gilman Drive, Mail Code 0448, La Jolla, CA 92093-0448, United States

HIGHLIGHTS

- Encapsulating organic thin-films improves stretchability by suppressing cracking.
- Model shows encapsulation delocalizes strain around film defects.
- First solar cell with intrinsic stretchability in all components is demonstrated.

GRAPHICAL ABSTRACT

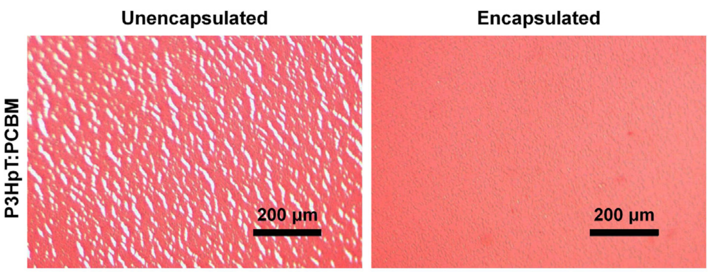

ARTICLE INFO

Article history:
Received 28 October 2015
Received in revised form 18 February 2016
Accepted 18 March 2016
Available online 22 March 2016

Keywords:
Stretchable solar cell
Stretchable electronics
Organic solar cell
Encapsulation
P3HpT
Crack-onset strain

ABSTRACT

This paper describes a large increase in the stretchability – i.e., resistance to cracking under tensile deformation – of organic semiconductor films produced by encapsulation. Specifically, encapsulation is shown to greatly suppress crack formation and growth in films of materials relevant to organic solar cells. Encapsulated films of the organic bulk heterojunction blend of poly(3-heptylthiophene) and phenyl-C_{61}-butyric acid methyl ester (P3HpT:PCBM) exhibit greater crack-onset strain, lower crack density, and lower average crack length than unencapsulated films. Films of P3HpT:PCBM on polyurethane (PU) showed cracks at $6.6 \pm 0.5\%$ without encapsulation and $40 \pm 4\%$ with encapsulation. Films of the conductive polymer poly(3,4-ethylenedioxythiophene):poly(styrenesulfonate) (PEDOT:PSS) also demonstrate suppressed cracking when encapsulated, as well as reduced dependence of resistance on strain after the crack-onset strain (which indicates a greater usable range of strain for encapsulated vs. unencapsulated films). A finite element model is used to explain the mechanism suppressing crack growth, which involves delocalization of strain around minor defects in the films by the encapsulating substrate. In addition, encapsulation is used to enable the first encapsulated solar cell in which every component is intrinsically stretchable. These cells are stretchable to 9–10% strain, with some cells performing well even after their crack-onset strain of 8–9%, whereas unencapsulated cells fail at 4% strain. This work highlights the necessity to consider encapsulation – already

* Corresponding author.
E-mail address: dlipomi@ucsd.edu (D.J. Lipomi).

http://dx.doi.org/10.1016/j.eml.2016.03.012
2352-4316/© 2016 Elsevier Ltd. All rights reserved.

important for protecting the electronically active components of a device from abrasion, weathering, or chemical damage – as an important factor in the mechanical robustness of stretchable devices.

© 2016 Elsevier Ltd. All rights reserved.

1. Introduction

Intrinsically stretchable electronics have the potential to enable applications where robustness and repeatable stretchability, in addition to flexibility, are required. Possible applications where stretchable materials would have a large benefit include soft robotics [1,2], electronic skins [3,4] and other bio-integrated devices [5], and devices that require rough or frequent handling, such as portable or foldable solar cells [6,7] or electronics incorporated into textiles [8,9]. In addition, manufacturing using roll-to-roll processes [10] also involves significant mechanical stress that can lead to cracking and delamination [11]. Common and highly successful approaches to producing stretchable devices include deterministic patterning of serpentine structures that accommodate global tensile strains by local bending strains [12,13] or pre-straining the substrate to induce buckling in the active layers [14–17]. An alternative, complementary approach would be to produce electronic devices in which every component – the substrates, the electrodes, the interconnects, and the semiconductors – were intrinsically stretchable, that is, exhibited reversible deformability over a large range of strain using all organic materials [18,19]. This approach might facilitate manufacturing (i.e., all components could be printed) for some applications, such as mechanically robust solar modules and wearable sensors.

The mechanical properties of intrinsically – or "molecularly" – stretchable electronic materials, such as organic conductors and semiconductors, are generally measured with the material as a thin film sitting atop an elastic substrate [20]. With such supported films, it is possible to measure the tensile modulus and to estimate the strain at fracture by measuring the strain at which the first crack appears (crack-onset strain). While this technique for measuring the ductility is useful for comparing the relative mechanical stability of two materials, it represents an unlikely scenario in a real-world device, since these ultra-compliant devices will be encapsulated. This paper describes a large increase in stretchability – i.e., a dramatic suppression of cracking – obtained by encapsulating conjugated polymer films and whole devices in thermoplastic polyurethane (Fig. 1). To understand the mechanism behind the enhancement in stretchability, we used a finite element model to simulate the localization of strain around a variety of types of film defects. Finally, we demonstrated an encapsulated organic solar cell with increased ability to survive damage by stretching.

2. Background

Some organic materials have demonstrated high degrees of mechanical compliance and tolerance to high strains as either the conducting [21,22] or semiconducting layers of devices [20,23]. Combining multiple stretchable components into a fully stretchable device, however, remains challenging. Much of the work in the field of stretchable organic electronics has been focused on molecular properties of single materials or device components [24–28], but device-level properties, such as interlayer adhesion, can also have a large effect on the mode and severity of device failure [29–32]. Adhesion plays an important role in the response of thin films to strain. For well adhered films, strain of the substrate imposes relatively uniform strain on the entire film – including at thin areas and defects – and thus the global strain determines the local strain. In contrast, in poorly adhered films, strain localizes to defects and thin areas, and this localization produces cracks at smaller strains than would be observed for well adhered films. Lu et al. demonstrated this effect by stretching copper films on Kapton substrates and found that, with an adhesion-enhancing chromium interlayer, the films were plastically deformable up to 52%, whereas films without the adhesion layer cracked around 30% strain [33]. Organic films have also demonstrated superior crack resistance with greater adhesion, as demonstrated by the improvement in the crack-onset strain in poly(3-hexylthiophene): [6,6]-phenyl-C_{61}-butyric acid methyl ester (P3HT:PCBM) films with a layer of poly(3,4-ethylenedioxythiophene):poly(styrene sulfonate) (PEDOT:PSS) acting as an adhesion layer [34]. Additionally, our laboratory previously found that the crack-onset strain of films of poly(3-dodecylthiophene) (P3DDT) was lower than films of poly(3-octylthiophene) (P3OT) on a poly(dimethylsiloxane) (PDMS) substrate, which we attributed to the relatively poorer adhesion of P3DDT than P3OT to the PDMS [20].

We thus hypothesized that encapsulation of organic semiconductor films would improve mechanical robustness by redistributing and minimizing local strain around defects. That is, the encapsulant and the substrate would act in concert to suppress the formation and propagation of cracks, in the same way as does a well adhered substrate acting alone. These effects would thus result in delayed onset and lower severity – i.e., lengths, density, or both – of cracks in elastic films under strain and in better performance of stretchable devices.

3. Experimental design

3.1. Selection of materials

To test the effects of encapsulation on a variety of stretchable films, we chose to strain the conductive polymer PEDOT:PSS strongly plasticized with a fluorosurfactant, a bulk heterojunction composite comprising P3HpT

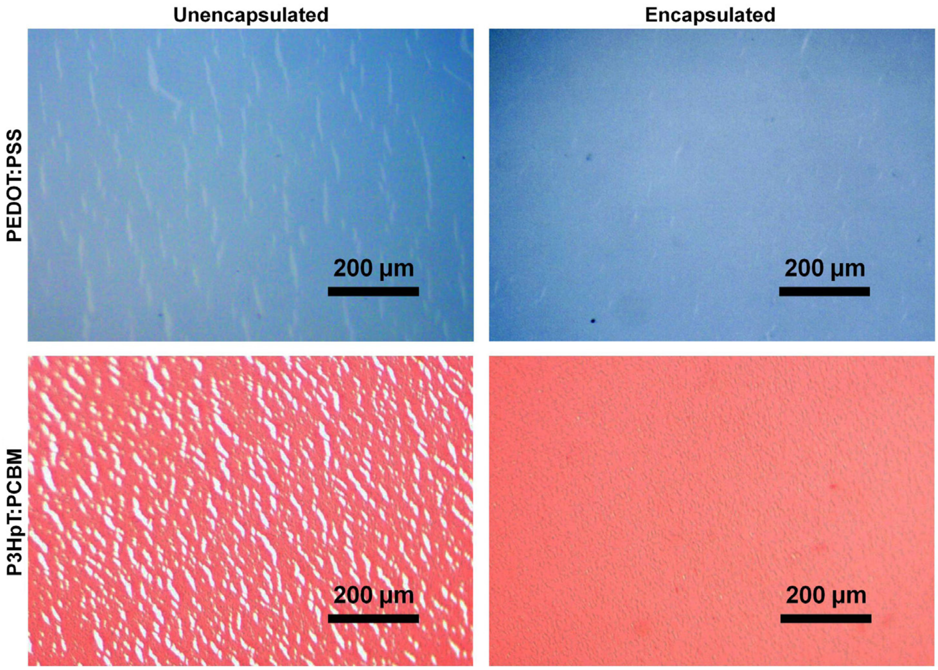

Fig. 1. Optical micrographs of strained poly(3,4-ethylenedioxythiophene):poly(styrene sulfonate) (PEDOT:PSS, top) and poly(3-heptylthiophene): [6,6]-phenyl-C_{61}-butyric acid methyl ester (P3HpT:PCBM, bottom) films, showing the difference between encapsulated (right) and unencapsulated (left) samples. The samples were all strained to 50%. A few short cracks (light lines or pinholes) are visible in the encapsulated samples, while the unencapsulated samples show catastrophic damage.

and PCBM, and an organic solar cell comprising components that are all stretchable. We selected PEDOT:PSS as our organic conductor because of its high conductivity and high crack onset strain when plasticized with a fluorosurfactant [21]. Use of poly(ethyleneimine) (PEI) to lower the work function permits PEDOT:PSS to be used as both the anode and cathode [35]. In addition, PEDOT:PSS has been previously demonstrated to be an effective stretchable anode in stretchable solar cells that employed a liquid metal cathode (top contact) [17,34].

We selected P3HpT:PCBM as the active layer because P3ATs are the most studied family of conjugated polymers and their blends with PCBM can produce solar cells with efficiencies up to 5% [36]. They also exhibit a high degree of mechanical compliance depending on the length of their alkyl side chain (the longer the side chain, the lower the tensile modulus and greater the ductility) [20]. In particular, P3HpT co-optimizes electronic performance (as manifested in the power conversion efficiency of a photovoltaic device) and mechanical compliance, owing to its glass transition temperature (T_g); P3HpT is the first in the series of P3ATs with increasing side chain whose T_g is significantly below room temperature, and can thus be considered a semiconducting thermoplastic elastomer [37].

Polyurethane (PU) was selected as the substrate because dip coating it onto glass slides produced substrates that were transparent, stretchable by many times their original length, and of controllable thickness ($\sim$150 μm thick on average in this study). In addition, its high surface energy (relative to PDMS) [38,39] enabled films to be easily adhered and transferred from hydrophobic glass slides. The high surface energy and viscoelasticity also promoted interlayer adhesion between it and the active film, thus delaying the crack onset of the films relative to those transferred onto a substrate with a lower surface energy, such as PDMS.

3.2. Testing mechanical properties

We conducted crack-onset strain studies of PEDOT:PSS and P3HpT:PCBM bonded to PU substrates, as opposed to pull testing of bulk samples of conjugated polymers, for the sake of simplicity and because thin films on elastic substrates represented a closer approximation of a real-world device. In addition, the film-on-elastomer system allows characterization of the cracking behavior of the system from zero strain until well after the crack onset strain [21]. The use of a linear actuator ensured that the strain rate was applied uniformly across all samples. For Sections 4.1 and 4.2, one unencapsulated and one encapsulated sample were taken from each as-cast film to mitigate the effects of sample-to-sample variation. Solar cells were strained using a purpose-built stage in a nitrogen-filled glove box during testing to minimize oxidation.

4. Results and discussion

4.1. Cracking properties of P3HpT:PCBM

To explore the effects of encapsulation on semiconducting films under strain, we measured the crack-onset strain, average crack density at 50% strain, and average

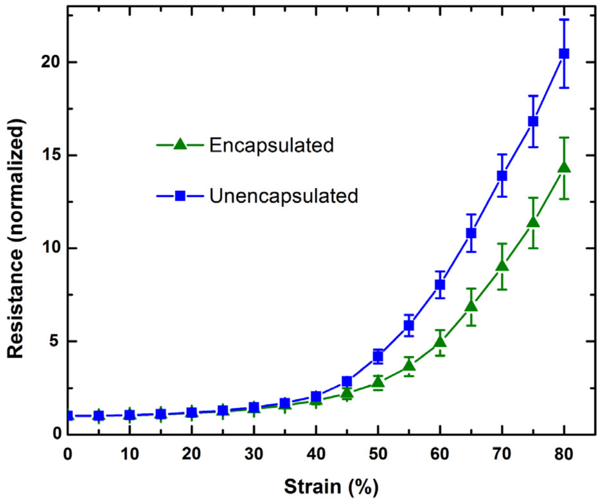

Fig. 2. Evolution of resistance vs. strain for PEDOT:PSS films, showing differences between encapsulated and unencapsulated samples. Encapsulation reduced damage due to cracking, though there was still significant reduction in performance above 50% strain.

crack length at 50% strain. Films of P3HpT:PCBM on PU showed cracks at 6.6 ± 0.5% without encapsulation and 40 ± 4% with encapsulation. In addition, cracks in the unencapsulated films were large and clearly visible right after the crack-onset strain, while those in encapsulated films were very small, pinhole cracks (Fig. 1). The crack densities of the unencapsulated films and encapsulated films at 50% strain were 890 ± 80 and 46 ± 6 cracks mm^{-2}, while the average crack lengths were 27 ± 4 and 9.2 ± 0.7 μm, respectively. Overall, these values demonstrate a strong suppression of cracks in this material due to encapsulation.

4.2. Electrical response of encapsulated PEDOT:PSS to strain

To quantify the evolution of electrical conductivity of thin stretchable films with strain, we measured the resistance of both unencapsulated and encapsulated PEDOT:PSS films from 0% to 80% strain (Fig. 2). Below 35% strain, the films followed identical trends, but as cracks began to appear, the resistance of the unencapsulated sample increased rapidly. Above 50% strain, the conductivity of both the encapsulated and unencapsulated samples decreased rapidly with increasing strain. We attribute this decrease in conductivity to cracks that appeared in the films. The unencapsulated PEDOT:PSS had a crack-onset of 38.4% ± 1.4%, while encapsulation slightly delayed the crack-onset to 41.4% ± 0.6%. Encapsulation also significantly inhibited the ability of the cracks to grow, resulting in shorter cracks and more percolated pathways to maintain electrical conductivity. We measured crack density at 50% strain (Fig. 1) to be roughly the same for the unencapsulated and encapsulated samples (99 ± 13 vs. 91 ± 22 cracks mm^{-2}, respectively), but the cracks in the unencapsulated sample were much longer on average (89 ± 10 μm vs. 43 ± 4 μm for the encapsulated sample). The crack density varied significantly between samples, possibly due to slight differences in strain rate, air temperature, humidity, or other processing conditions, but the cracks in the unencapsulated samples were uniformly longer.

4.3. Simulations of strain delocalization by encapsulation

To investigate the mechanism responsible for the improved robustness of encapsulated films, we performed finite element analysis. Localization of strain, which leads to crack formation and propagation, occurs where a small defect has formed in the fabrication process or general use of the device. We therefore introduced several types of defects into the simulation: a small crack perpendicular to the direction of strain, a pinhole defect (circular hole through the film with diameter equal to one quarter the thickness of the film), and an area of thinning in the active layer of the device. The thin film was given the mechanical properties (tensile modulus, tensile strength, Poisson ratio, density) [40] of PEDOT:PSS, and the substrate and encapsulant were given those of PU [41].

As shown in Fig. 3(a)–(h) and Fig. 4, encapsulation greatly reduced the local strain near pinhole defects and microcracks in the device. Delamination also played a role, because defects in delaminated regions were less constrained than in regions adhered to the substrate, resulting in greater local strain. The strains were most delocalized when the films were adhered to both the bottom substrate and the top encapsulating substrate, producing local strains that were closer to the value of the overall strain (see Table 1; overall strain was 31%, see Section 6.6 for details). The simulations also support the hypothesis that there is a positive feedback loop between cracking and delamination. For example, the strain along the edge of an unencapsulated, non-delaminated crack (Fig. 3(a)) would likely lead to delamination of the film from the bottom substrate, since the strain is highest along the interface between the film and the substrate. This delamination would allow the crack to open, as in Fig. 3(c), and would result in further cracking of the film. Rows 2, 4, and 5 of Table 1 describe the strain in the active film in areas likely to delaminate from one of the substrates, since these points are offset from the defect in the direction of strain. In addition, when the local strain is high in these locations, it tends

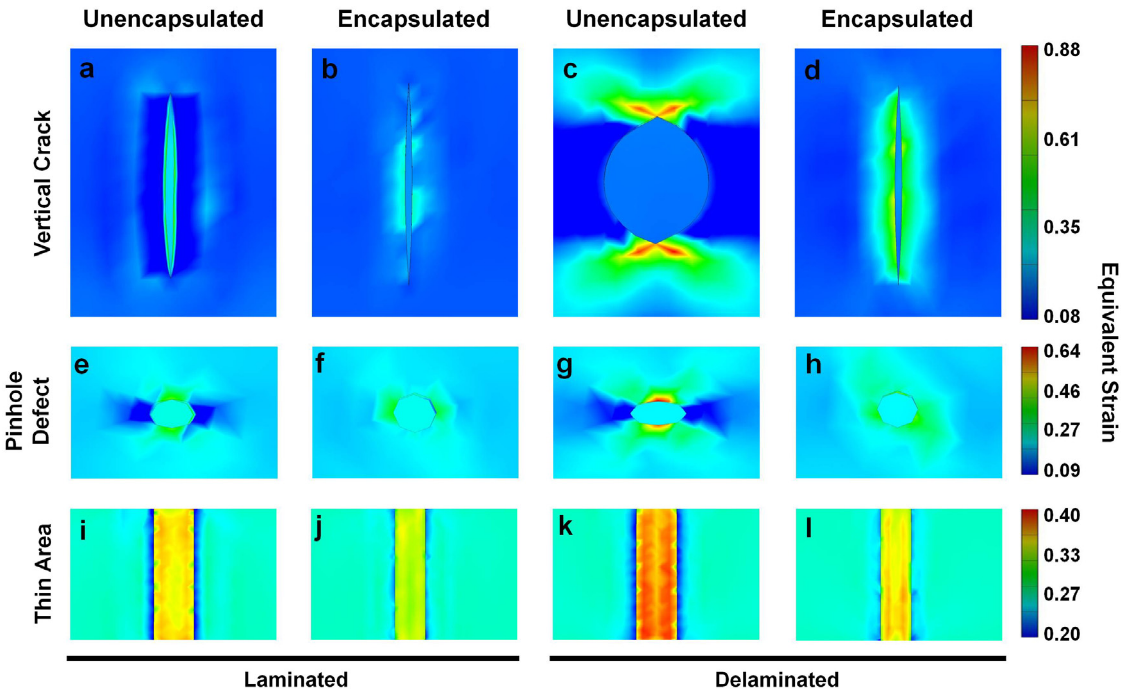

Fig. 3. Finite element analysis results showing encapsulation suppressing cracking by strain delocalization. The first and third columns show the simulation of unencapsulated samples (a, c, e, g, i, and k), while the second and fourth columns show the simulation of encapsulated samples (b, d, f, h, j, and l), with the encapsulating layer made invisible for the figure. Each row shows the effect of a different defect on the film: a thin vertical crack (a–d), a small pinhole defect (e–h), and an area of local thinning (i–l). The first two columns compare unencapsulated and encapsulated films which are laminated to the substrate (a, b, e, f, i, and j), while the third and fourth columns compare unencapsulated and encapsulated films which are delaminated from the substrate (c, d, g, h, k, and l). All delaminated defects produce higher local strain than the laminated defects. Maximum local strain is reduced by encapsulation in all cases (see Table 1). The total strain along the horizontal axis is 31.0%.

Table 1
Equivalent strains near the defects shown in Fig. 3. Strain around the defects of films adhered to both a bottom and an encapsulating substrate was most delocalized, with all local strains closer to the overall strain of 31.0%, than the strains of corresponding defects for the other conditions.

Location and defect type	Unencapsulated	Encapsulated	Unencapsulated, with delamination	Encapsulated, with delamination
1. Tip, vertical crack	0.303	0.288	0.873	0.318
2. Next to edge, vertical crack	0.653	0.432	0.274	0.684
3. Top edge of pinhole, perpendicular to strain	0.452	0.314	0.639	0.347
4. Left edge of pinhole, parallel with strain	0.088	0.411	0.112	0.435
5. Inside edge of pinhole	0.438	0.226	0.121	0.185
6. Thin area	0.364	0.351	0.383	0.369

to be highest at the interface between the film and one of the substrates, and it falls off rapidly away from the interface. The areas described by rows 1, 3, and 6, on the other hand, are likely to crack before delaminating, since they are offset from the defect perpendicular to the direction of strain. This offset is in the direction in which cracks generally propagate after initial formation. We also simulated a film with no defects other than a small area of delamination, but there was no localization of strain due to the unbroken symmetry of the substrate and thin film.

4.4. *Performance of encapsulated, stretchable solar cell and evolution with strain*

To demonstrate the improved robustness of these encapsulated films, we fabricated encapsulated, stretchable solar cells with the following architecture: PU/PEDOT:PSS/PEI/P3HpT:PCBM/PEDOT:PSS/PU (Fig. 5). The encapsulated devices showed a crack-onset strain of 8%–9%, a large increase over the unencapsulated devices, which cracked after only 3%–4% strain (Fig. 6). Though the crack-onset strains of encapsulated layers of PEDOT:PSS and P3HpT:PCBM were both approximately 40%, the incorporation of the PEI layer, as well as the added complexity of the complete device (e.g., more chances for defects to occur and more interfaces at which delamination can occur), had the effect of greatly reducing the stretchability of the complete device. Until the devices cracked, however, they showed little degradation in performance with strain (Fig. 7). After cracking, the short circuit current of most devices fell rapidly due to the increase in series resistance of the PEI-modified contact, though some cells continued to

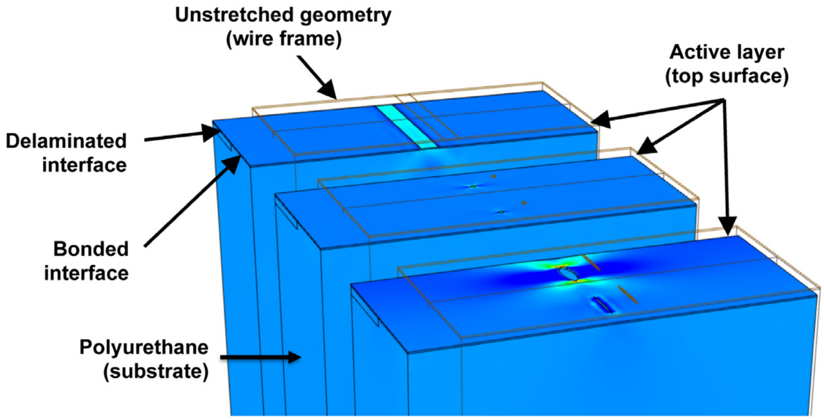

Fig. 4. Side view showing the structures simulated in Fig. 3 (for clarity, the figure shows unencapsulated devices only, i.e., Fig. 3(a), (c), (e), (g), (i), (k)). Encapsulated structures (i.e., Fig. 3(b), (d), (f), (h), (j), (l)) would have another thick layer of polyurethane on top of the active layer.

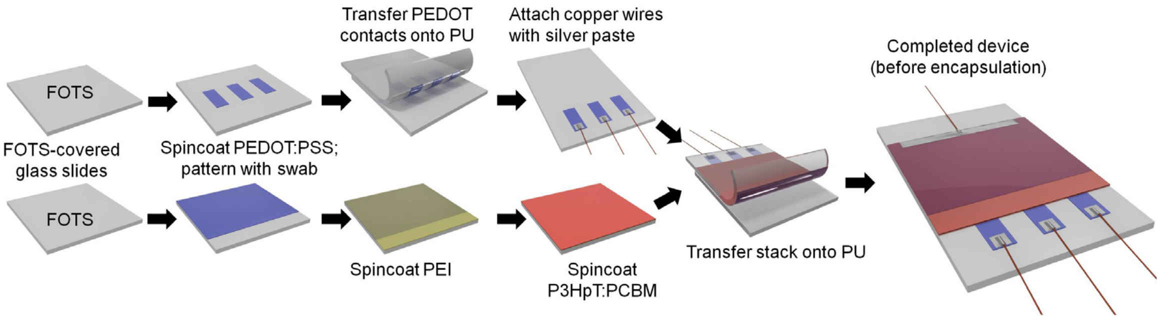

Fig. 5. Diagram of cell architecture and fabrication. PEDOT:PSS top and bottom contacts were spin-coated on separate glass slides treated with tridecafluoro-1,1,2,2-tetrahydrooctyl trichlorosilane (FOTS) and patterned with damp swabs. PEI was spin-coated on the eventual top contact, followed by P3HpT:PCBM. All layers were annealed as described in the methods section. The bottom contacts were transferred to the PU substrate and wires were attached. A second transfer lifted the top contact, the PEI, and the active layer together off the second FOTS-coated slide. Finally, a wire was added to the top contact and the device was complete, with encapsulation to enhance stretchability then optional.

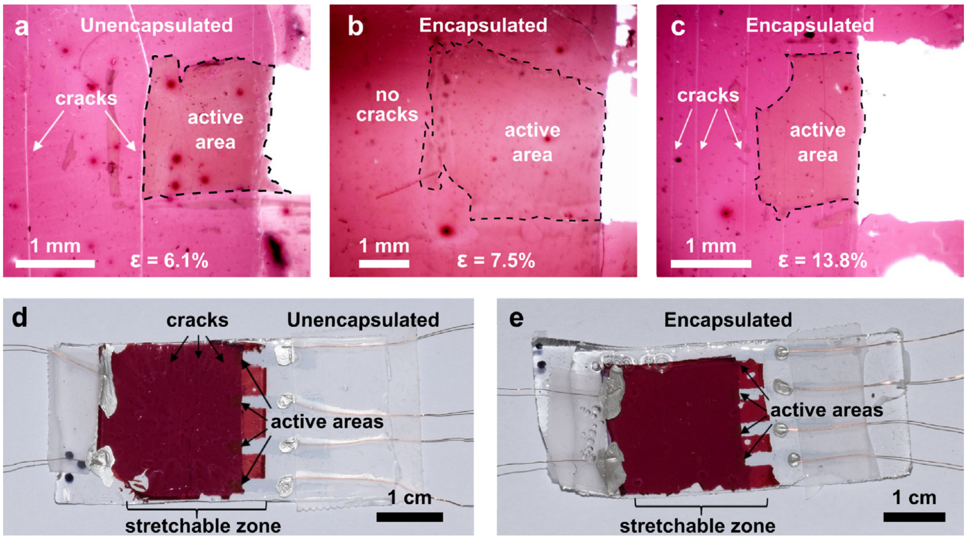

Fig. 6. Pictures of the solar cells. a: active area of an unencapsulated device, strained to 6.1%. b: active area of an encapsulated device, strained to 7.5%. c: active area of an encapsulated device, strained to 13.8%. d and e: unencapsulated and encapsulated devices, after straining to 6.1 and 13.8%, respectively (same samples as a and c). Long, catastrophic cracks can be seen in a, c, and d, and also exist in e (visible with microscope, as in c, but not in this picture), but do not exist in b. The active areas are visible as dark patches near the centers of d and e, with the small PEDOT:PSS contacts extending rightward to where the wires are attached with silver paint. The notched pattern on the right side of the devices is produced during the transfer of the active layer and PEI-modified electrode, but the areas left behind in the transfer are not necessary for the device.

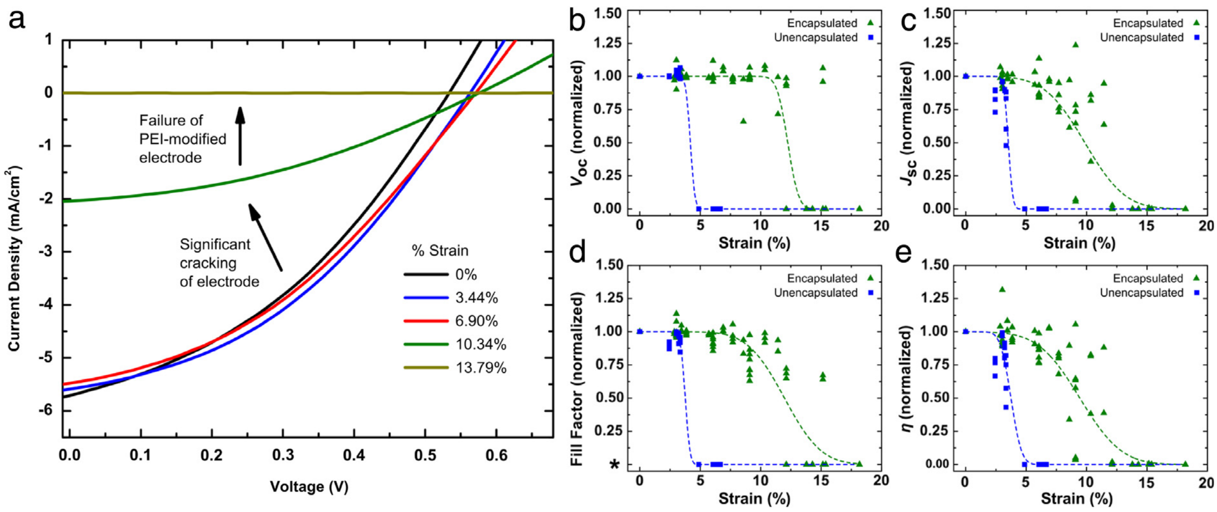

Fig. 7. Evolution of the response of the solar cells with strain. Plot a is a representative JV curve of an encapsulated, stretchable solar cell. Cracking began at 8%–9% strain, followed by complete failure around 13% strain. Just after the crack-onset strain, the cracking was localized to only one area in some devices, allowing some cells to perform at levels close to their initial performance even past 10% strain. Others, such as this one, saw a marked increase in series resistance due to the cracking of the PEI-modified electrode. Plots b through e show the evolution of the figures of merit, showing failure of the unencapsulated cells at much lower strain. In d, total loss of functionality is plotted at zero (*). The fits in b–e are to the function $f(x) = 0.5\mathrm{erf}[ax + b] + 1$, where $\mathrm{erf}(x)$ is the error function, and are for visual effect only. The device which produced plot a is shown in Fig. 5(c) and (e), and has fill factor 0.40 and efficiency (h) 1.25%.

output power when cracks did not appear globally in the films. Multiple cells were thus able to perform above 80% of their initial efficiencies past 10% strain. Unlike the single films, the complete devices exhibited cracks which ran across most of the length of the films, consistent with a significant increase in brittleness due to the PEI [21]. There was little to no leakage current due to the cracks (which was a significant problem for cells made with a liquid metal top contact [34]), as there was little change in the negative bias dark current and virtually no change in open circuit voltage until total failure of the devices. The fill factor remained constant until the series resistance increased greatly due to cracking and turned the entire solar response curve linear. We note that these effects were measured for uniaxial deformation only and did not test the effects of biaxial loading. Orthogonal axes cannot however be strained independently, and it is likely that stretching along an axis orthogonal to the first stretched axis would produce cracks at smaller strains than were measured for unstretched films.

We note that the power conversion efficiencies of the devices of ∼1.25% are not competitive with the state of the art in the literature. While the open-circuit voltages are typical of P3AT:PCBM devices, the fill factors and short-circuit current density are low. The low fill factor and current was clearly influenced in part by a high series resistance, which was consistent with the use of PEDOT:PSS as both the anode and cathode, which has significantly lower conductivity than ITO and evaporated metal contacts, such as aluminum or silver. We cannot rule out possible detrimental effects of the multiple manipulations required to transfer the active layer and contacts from passivated glass slides to the elastomeric polyurethane, which could potentially introduce defects and thin areas and decrease the parallel (shunt) resistance, and thus the fill factor. The development of high-conductivity stretchable transparent electrodes might reduce losses associated with series resistance (and thus fill factor) while developing new crosslinked elastomers might permit the direct casting of organic electronic materials from solution to avoid potential damage caused by mechanical transfer of the layers.

5. Conclusions

We demonstrated that encapsulation increases the mechanical robustness of stretchable thin films and devices by delocalizing strain around defects and suppressing crack formation and growth. This increased robustness was observed in conjugated polymer films, as well as in the first encapsulated, stretchable solar cells, i.e., solar cells in which all layers, including the substrate, encapsulant, and both electrodes, were intrinsically stretchable. We expect these results to be applicable to a wide variety of materials, making them relevant for a range of applications involving stretchable thin films and stretchable electronics in general. As we only tested the effects of encapsulation by polyurethane, however, future studies could determine if the effect is enhanced by tailoring the properties of the encapsulant (e.g., adhesion, elastic modulus, Poisson ratio, strength, and toughness) to provide the maximum increase in robustness given the specific properties of the encapsulated film or device. For the encapsulated, stretchable solar cell, significant enhancement in both stretchability and efficiency should be made possible by further study of stretchable semiconducting and conducting materials, especially the development of stretchable conductors with work functions differing from that of PEDOT:PSS.

6. Experimental methods

6.1. Materials

Poly(3-heptylthiophene) was purchased from Rieke Metals, Inc., and used as received. [6,6]-phenyl C_{61} butyric acid methyl ester (PCBM) was obtained from Sigma-Aldrich with >99% purity. Polyurethane (PU, Tecoflex SG-80A, kindly donated by Lubrizol) was used as received. (Tridecafluoro-1,1,2,2-tetrahydrooctyl)-1-trichlorosilane (FOTS) was obtained from Gelest. PEDOT:PSS (Clevios PH1000) was purchased from Heraeus. DMSO was purchased from BDH with purity of 99.9% and Capstone (FS-30) fluorosurfactant were purchased from Sigma-Aldrich. Polyethylenimine (PEI), Ortho-dichlorobenzene (ODCB), acetone, isopropyl alcohol (IPA), ethanol, and tetrahydrofuran (THF) were obtained from Sigma-Aldrich and used as received.

6.2. Preparation of substrates

Glass slides were cut with a diamond-tipped scribe into 2.5 cm squares for spin coating, or 5×2.5 cm rectangles for fabrication of PU substrates. They were then subsequently cleaned with Alconox solution (2 mg mL^{-1}), deionized water, acetone, and then isopropyl alcohol (IPA) in an ultrasonic bath for 10 min each and then rinsed and dried with compressed air. Next, the glass was plasma treated at ~30 W for 3 min at a base pressure of 200 mtorr ambient air to remove residual organic material and activate the surface. They were then enclosed in a vacuum desiccator with a vial containing ca. 100 μL FOTS and left under dynamic vacuum for 3 h. The FOTS-treated glass slides were rinsed with isopropanol and dried under a stream of compressed air before use.

PU substrates were fabricated by dip coating 5×2.5 cm glass slides, treated with FOTS, into an 18% PU solution in tetrahydrofuran (THF). The slides were dried for at least 3 h in a fume hood, and then overnight in a vacuum oven to remove residual THF. The resulting substrates are clear, smooth, and stretchable to hundreds of percent strain, and about 150 μm thick, on average. For the resistance vs. strain and crack-onset studies, the substrates were then cut in half to create 1.25×5 cm strips.

6.3. Resistance vs. strain and crack-onset studies

To increase the conductivity and stretchability of our PEDOT:PSS solution we added 7% DMSO and 16% Capstone FS-30, respectively. The latter is a replacement for Zonyl FS-300 (recently out of production), which greatly enhances the mechanical compliance of the films [21]. The PEDOT:PSS solution was spin coated on FOTS treated 2.5×2.5 cm glass slides (120 s at 500 RPM, 30 s at 2000 RPM), and annealed on a hot plate for 30 min at 100 °C. They were then transferred to 1.25×5 cm PU strips by conformably adhering the strips on half of the slide, applying gentle pressure, and gently removing the PU, thus lifting off the PEDOT:PSS film as well. Leads were then attached by silver paint on the ends of the strips. Once the silver paint was dry the strips were either encapsulated, with another strip of PU applied in the same way, or left unencapsulated. They were then strained on a linear actuator at a rate of roughly a few percent per min, though extra time was needed before measurements were made to allow the resistance values to stabilize. While we did not measure the effect of strain rate on the cracking behavior, our experience leads us to believe that significantly greater rates of strain would lead to greater effective brittleness, as is common for polymeric materials.

P3HpT:PCBM (40 mg/mL solution in ODCB, allowed to stir overnight and filtered with a 1-μm glass microfiber (GMF) syringe filter) was spin coated on FOTS treated 2.5×2.5 cm glass slides (240 s at 500 RPM, 30 s at 2000 RPM). They were then annealed on a hot plate in a glove box for 25 min at 110 °C and allowed to slowly cool on the hot plate. They were then transferred in the same manner as the PEDOT:PSS films, encapsulated or left unencapsulated, and strained using a computer-controlled linear actuator at a rate of about two to three percent per min. At each step, optical micrographs were taken to observe the film surfaces. The crack-onset strains were defined by the strain at which the first crack was observed by optical microscopy.

6.4. Fabrication of encapsulated, stretchable solar cells

Fully stretchable solar cells were composed of a P3HpT:PCBM active layer and two electrodes of PEDOT:PSS, one of which having been modified with PEI to lower its work function [35,42,43]. Solar cells were fabricated by sequentially spin coating two layers of PEDOT:PSS (16% Capstone FS-30, 7% DMSO, 500 rpm for 120 s and 2000 rpm for 30 s, annealed at 100 °C for 10 min after each coating), PEI (0.55% solution in ethanol, 3000 rpm for 30 s, annealed at 100 C for 10 min), and P3HpT:PCBM (40 mg mL^{-1} in ODCB, 500 rpm for 240 s and 2000 rpm for 30 s, annealed for 25 min in a nitrogen filled glove box) on an FOTS coated 2.5×2.5 cm glass slide. It was found that the PEI layer negatively impacted the conductivity of the PEDOT:PSS if only one layer was used, but the problem was solved by spin-coating an additional layer of PEDOT:PSS before spin-coating the PEI on top. The transparency of this contact was not problematic since it was not the transparent electrode in our device architecture. Before spinning the PEI, a small strip of the PEDOT:PSS was removed with a wet swab to avoid effects arising from inhomogeneities in thickness and coverage at the edge of the film. Ethanol was used for the PEI solution because spinning a methoxyethanol solution on PEDOT:PSS dramatically reduces the stretchability of the film (possibly due to extraction of the fluorosurfactant plasticizer) [21]. While the PEI spun out of ethanol still embrittles the films, the catastrophic failure observed when spinning PEI out of methoxyethanol does not occur.

The other contacts were created by spin coating PEDOT:PSS (same parameters as above, but only a single layer) on a separate FOTS coated glass slide, patterning the film into contacts with a damp swab, annealing as above, and then transferring the contacts to a 5×2.5 cm PU strip as described in the previous section. Silver paint was used to attach leads to the PEDOT:PSS strips, and the contacts and paint were further dried in under vacuum for 5 min. The active layer and second electrode were then transferred in the same manner, with the areas of the solar cells determined by the alignment of the smaller PEDOT contacts and the swabbed edge of the other (PEI modified) PEDOT layer. Silver paint was added to attach leads to the top contact, and the device was moved into a nitrogen filled glove box for testing. If the device was encapsulated, another layer of the PU substrate was placed on the device and adhered with gentle pressure.

6.5. Photovoltaic measurements

We performed all photovoltaic measurements in a nitrogen filled glovebox using a solar simulator approximating the AM 1.5 G spectrum with a flux of 100 mW/cm^2 (ABET Technologies 11016-U up-facing unit calibrated with a reference cell with a KG5 filter). The current density versus voltage was measured using a Keithley 2400 SourceMeter. Samples were strained in the glove box by a purpose-built stage for holding and straining the devices [17]. The open circuit voltages and fill factors of the cells are independent of areas of the cells, but the currents and efficiencies were normalized to take the strain into account.

6.6. Computational modeling of strain

In order to obtain the strain distribution maps of the PEDOT thin films on polyurethane (PU) under tension with and without encapsulation with PU, computer-assisted design (CAD) models of the geometries were created in Autodesk Inventor 2016 with the corresponding material parameters applied to all parts. The part dimensions in the model were as follows: the PEDOT film was $0.2 \times 20 \times 40$ μm, the PU substrate was $60 \times 20 \times 40$ μm, and the encapsulating PU was $10 \times 20 \times 40$ μm. We reproduced 3 sets of equivalent assemblies and introduced "defects" into the PEDOT film of each assembly: two of each kind—point defects, cracks (symmetrically located with respect to the delaminated/non-delaminated film boundary), and film thinning (areas of the film with a thickness of only 75% of the bulk film thickness) spanning the width of the assembly. Each assembly set bore one kind of a defect. The layers were stacked accordingly with interfaces simulated as "bonded", except the delaminated areas of the PEDOT/PU substrate interface was simulated as "sliding no separation". A static linear finite element analysis (FEA) simulation of the stretching of the assembly to 31.0% strain was then performed. This choice of strain in all simulations corresponds to the arbitrarily selected force required to generate adequate strain in the first simulation and was subsequently used for the rest of the simulations; the trends in the localization of strain near the defects, however, do not depend on the choice of overall strain. The mesh size was selected as the 0.05 fraction of the smallest dimension of a part, while the minimal element size as the 0.1 fraction of the mesh size. The constraints were the following: one end of the assembly (as described by rectangles formed by thickness and width of parts) was fixed with zero degrees of freedom, while the opposite end of the assembly was displaced (with one degree of freedom) by 12.38 μm inducing 31.0% strain.

Acknowledgments

This work was supported by the Air Force Office of Scientific Research (AFOSR) Young Investigator Program, grant number FA9550-13-1-0156. A. V. Z. was supported by the National Science Foundation Graduate Fellowship Program under Grant No. DGE-1144086. A. B. acknowledges support from the Calit2 High School Summer Scholars Program at UCSD.

References

[1] R.F. Shepherd, F. Ilievski, W. Choi, S.A. Morin, A.A. Stokes, A.D. Mazzeo, et al., Multigait soft robot, Proc. Natl. Acad. Sci. 108 (2011) 20400–20403. http://dx.doi.org/10.1073/pnas.1116564108.
[2] G. Kofod, W. Wirges, M. Paajanen, S. Bauer, Energy minimization for self-organized structure formation and actuation, Appl. Phys. Lett. 90 (2007) 081916. http://dx.doi.org/10.1063/1.2695785.
[3] G. Buchberger, R. Schwödiauer, S. Bauer, Flexible large area ferroelectret sensors for location sensitive touchpads, Appl. Phys. Lett. 92 (2008) 123511. http://dx.doi.org/10.1063/1.2903711.
[4] M. Kaltenbrunner, T. Sekitani, J. Reeder, T. Yokota, K. Kuribara, T. Tokuhara, et al., An ultra-lightweight design for imperceptible plastic electronics, Nature 499 (2013) 458–463. http://dx.doi.org/10.1038/nature12314.
[5] M.L. Hammock, A. Chortos, B.C.-K. Tee, J.B.-H. Tok, Z. Bao, 25th anniversary article: The evolution of electronic skin (e-skin): a brief history, design considerations, and recent progress, Adv. Mater. 25 (2013) 5997–6038. http://dx.doi.org/10.1002/adma.201302240.
[6] F.C. Krebs, T.D. Nielsen, J. Fyenbo, M. Wadstrøm, M.S. Pedersen, Manufacture, integration and demonstration of polymer solar cells in a lamp for the "Lighting Africa" initiative, Energy Environ. Sci. 3 (2010) 512–525. http://dx.doi.org/10.1039/b918441d.
[7] M. Kaltenbrunner, M.S. White, E.D. Głowacki, T. Sekitani, T. Someya, N.S. Sariciftci, et al., Ultrathin and lightweight organic solar cells with high flexibility, Nature Commun. 3 (2012) 770. http://dx.doi.org/10.1038/ncomms1772.
[8] A. Bedeloglu, A. Demir, Y. Bozkurt, N.S. Sariciftci, A flexible textile structure based on polymeric photovoltaics using transparent cathode, Synth. Met. 159 (2009) 2043–2048. http://dx.doi.org/10.1016/j.synthmet.2009.07.019.
[9] F.C. Krebs, M. Biancardo, B. Winther-Jensen, H. Spanggard, J. Alstrup, Strategies for incorporation of polymer photovoltaics into garments and textiles, Sol. Energy Mater. Sol. Cells 90 (2006) 1058–1067. http://dx.doi.org/10.1016/j.solmat.2005.06.003.
[10] F.C. Krebs, N. Espinosa, M. Hösel, R.R. Søndergaard, M. Jørgensen, 25th anniversary article: Rise to power—OPV-based solar parks, Adv. Mater. 26 (2014) 29–39. http://dx.doi.org/10.1002/adma.201302031.
[11] S.R. Dupont, M. Oliver, F.C. Krebs, R.H. Dauskardt, Interlayer adhesion in roll-to-roll processed flexible inverted polymer solar cells, Sol. Energy Mater. Sol. Cells 97 (2012) 171–175. http://dx.doi.org/10.1016/j.solmat.2011.10.012.
[12] D.S. Gray, J. Tien, C.S. Chen, High-conductivity elastomeric electronics, Adv. Mater. 16 (2004) 393–397. http://dx.doi.org/10.1002/adma.200306107.
[13] Y. Hattori, L. Falgout, W. Lee, S.-Y. Jung, E. Poon, J.W. Lee, et al., Multifunctional skin-like electronics for quantitative, clinical monitoring of cutaneous wound healing, Adv. Healthc. Mater. 3 (2014) 1597–1607. http://dx.doi.org/10.1002/adhm.201400073.
[14] D.-H. Kim, J.-H. Ahn, W.M. Choi, H.-S. Kim, T.-H. Kim, J. Song, et al., Stretchable and foldable silicon integrated circuits, Science 320 (2008) 507–511. http://dx.doi.org/10.1126/science.1154367.
[15] W.M. Choi, J. Song, D. Khang, H. Jiang, Biaxially stretchable wavy silicon nanomembranes, Nano Lett. 7 (2007) 1655–1663.
[16] J. Lee, J. Wu, M. Shi, J. Yoon, S.-I. Park, M. Li, et al., Stretchable GaAs photovoltaics with designs that enable high areal coverage, Adv. Mater. 23 (2011) 986–991. http://dx.doi.org/10.1002/adma.201003961.
[17] D.J. Lipomi, B.C.-K. Tee, M. Vosgueritchian, Z. Bao, Stretchable organic solar cells, Adv. Mater. 23 (2011) 1771–1775. http://dx.doi.org/10.1002/adma.201004426.

[18] S.M. Ha, W. Yuan, Q. Pei, R. Pelrine, S. Stanford, Interpenetrating polymer networks for high-performance electroelastomer artificial muscles, Adv. Mater. 18 (2006) 887–891. http://dx.doi.org/10.1002/adma.200502437.

[19] J. Liang, L. Li, X. Niu, Z. Yu, Q. Pei, Elastomeric polymer light-emitting devices and displays, Nat. Photonics 7 (2013) 817–824. http://dx.doi.org/10.1038/nphoton.2013.242.

[20] S. Savagatrup, A.S. Makaram, D.J. Burke, D.J. Lipomi, Mechanical properties of conjugated polymers and polymer-fullerene composites as a function of molecular structure, Adv. Funct. Mater. 24 (2014) 1169–1181. http://dx.doi.org/10.1002/adfm.201302646.

[21] S. Savagatrup, E. Chan, S.M. Renteria-Garcia, A.D. Printz, A.V. Zaretski, T.F. O'Connor, et al., Plasticization of PEDOT:PSS by common additives for mechanically robust organic solar cells and wearable sensors, Adv. Funct. Mater. 25 (2015) 427–436. http://dx.doi.org/10.1002/adfm.201401758.

[22] D.J. Lipomi, J.A. Lee, M. Vosgueritchian, B.C. Tee, J.A. Bolander, Z. Bao, Electronic properties of transparent conductive films of PEDOT:PSS on stretchable substrates, Chem. Mater. 24 (2012) 373–382.

[23] S. Savagatrup, A.D. Printz, H. Wu, K.M. Rajan, E.J. Sawyer, A.V. Zaretski, et al., Viability of stretchable poly(3-heptylthiophene) (P3HpT) for organic solar cells and field-effect transistors, Synth. Met. 203 (2015) 208–214. http://dx.doi.org/10.1016/j.synthmet.2015.02.031.

[24] O. Awartani, B.I. Lemanski, H.W. Ro, L.J. Richter, D.M. DeLongchamp, B.T. O'Connor, Correlating stiffness, ductility, and morphology of polymer: fullerene films for solar cell applications, Adv. Energy Mater. 3 (2013) 399–406. http://dx.doi.org/10.1002/aenm.201200595.

[25] S.R. Dupont, F. Novoa, E. Voroshazi, R.H. Dauskardt, Decohesion kinetics of PEDOT: PSS conducting polymer films, Adv. Funct. Mater. 24 (2014) 1325–1332. http://dx.doi.org/10.1002/adfm.201302174.

[26] N.R. Tummala, C. Risko, C. Bruner, R.H. Dauskardt, J.-L. Brédas, Entanglements in P3HT and their influence on thin-film mechanical properties: Insights from molecular dynamics simulations, J. Polym. Sci., Part B: Polym. Phys. 53 (2015) 934–942. http://dx.doi.org/10.1002/polb.23722.

[27] N.R. Tummala, C. Bruner, C. Risko, J.-L. Brédas, R.H. Dauskardt, Molecular-scale understanding of cohesion and fracture in P3HT: Fullerene blends, ACS Appl. Mater. Interfaces 7 (2015) 9957–9964. http://dx.doi.org/10.1021/acsami.5b02202.

[28] B. O'Connor, E.P. Chan, C. Chan, B.R. Conrad, L.J. Richter, R.J. Kline, et al., Correlations between mechanical and electrical properties of polythiophenes, ACS Nano 4 (2010) 7538–7544. http://dx.doi.org/10.1021/nn1018768.

[29] S.R. Dupont, E. Voroshazi, D. Nordlund, K. Vandewal, R.H. Dauskardt, Controlling interdiffusion, interfacial composition, and adhesion in polymer solar cells, Adv. Mater. Interfaces 1 (2014) 1400135. http://dx.doi.org/10.1002/admi.201400135.

[30] R.H. Dauskardt, M. Lane, Q. Ma, N. Krishna, Adhesion and debonding of multi-layer thin film structures, Eng. Fract. Mech. 61 (1998) 141–162.

[31] S.R. Dupont, E. Voroshazi, D. Nordlund, R.H. Dauskardt, Morphology and interdiffusion control to improve adhesion and cohesion properties in inverted polymer solar cells, Sol. Energy Mater. Sol. Cells 132 (2015) 443–449. http://dx.doi.org/10.1016/j.solmat.2014.09.013.

[32] S.R. Dupont, E. Voroshazi, P. Heremans, R.H. Dauskardt, Adhesion properties of inverted polymer solarcells: Processing and film structure parameters, Org. Electron. 14 (2013) 1262–1270. http://dx.doi.org/10.1016/j.orgel.2013.02.022.

[33] N. Lu, X. Wang, Z. Suo, J. Vlassak, Metal films on polymer substrates stretched beyond 50%, Appl. Phys. Lett. 91 (2007) 221909. http://dx.doi.org/10.1063/1.2817234.

[34] D.J. Lipomi, H. Chong, M. Vosgueritchian, J. Mei, Z. Bao, Toward mechanically robust and intrinsically stretchable organic solar cells: Evolution of photovoltaic properties with tensile strain, Sol. Energy Mater. Sol. Cells 107 (2012) 355–365. http://dx.doi.org/10.1016/j.solmat.2012.07.013.

[35] Y. Zhou, C. Fuentes-Hernandez, J. Shim, J. Meyer, A.J. Giordano, H. Li, et al., A universal method to produce low-work function electrodes for organic electronics, Science 336 (2012) 327–332. http://dx.doi.org/10.1126/science.1218829.

[36] J.Y. Kim, S.H. Kim, H.-H. Lee, K. Lee, W. Ma, X. Gong, et al., New architecture for high-efficiency polymer photovoltaic cells using solution-based titanium oxide as an optical spacer, Adv. Mater. 18 (2006) 572–576. http://dx.doi.org/10.1002/adma.200501825.

[37] S. Savagatrup, A.D. Printz, D. Rodriquez, D.J. Lipomi, Best of both worlds: Conjugated polymers exhibiting good photovoltaic behavior and high tensile elasticity, Macromolecules 47 (2014) 1981–1992. http://dx.doi.org/10.1021/ma500286d.

[38] D. Bodas, C. Khan-Malek, Formation of more stable hydrophilic surfaces of PDMS by plasma and chemical treatments, Microelectron. Eng. 83 (2006) 1277–1279. http://dx.doi.org/10.1016/j.mee.2006.01.195.

[39] C. Yao, J. Renzulli, G. Haleblian, T.J. Webster, Nanostructured polyurethane-poly-lactic- co-glycolic acid scaffolds increase bladder tissue regeneration? An in vivo study, Int. J. Nanomed. 8 (2013) 3285–3296.

[40] U. Lang, N. Naujoks, J. Dual, Mechanical characterization of PEDOT: PSS thin films, Synth. Met. 159 (2009) 473–479. http://dx.doi.org/10.1016/j.synthmet.2008.11.005.

[41] A. Marcos, Synthesis of HMDI-based segmented polyurethanes and their use in the manufacture of elastomeric composites, J. Biomater. Sci. Polym. Ed. 18 (2007) 561–578.

[42] T.F. O'Connor, A.V. Zaretski, B.a. Shiravi, S. Savagatrup, A.D. Printz, M.I. Diaz, et al., Stretching and conformal bonding of organic solar cells to hemispherical surfaces, Energy Environ. Sci. 7 (2014) 370–378. http://dx.doi.org/10.1039/c3ee42898b.

[43] W. Meng, R. Ge, Z. Li, J. Tong, T. Liu, Q. Zhao, et al., Conductivity enhancement of PEDOT: PSS films via phosphoric acid treatment for flexible all-plastic solar cells, ACS Appl. Mater. Interfaces 7 (2015) 14089–14094. http://dx.doi.org/10.1021/acsami.5b03309.